Metaheuristics-based approach for multiple dynamic responses optimization of flexible mechanisms

Mohamed Amine Ben Abdallah, Imed Khemili, Nizar Aifaoui, Med Amine Laribi

Metaheuristics based approach for multiple dynamic responses optimization of flexibles mechanisms

Mohamed Amine Ben Abdallah[1,2*], Imed Khemili[3], Nizar Aifaoui[2], Med Amine Laribi[4]

[1] Centre of Automotive Engineering, Department of Mechanical Engineering Sciences, Faculty of Engineering and Physical Sciences, University of Surrey, United Kingdom

[2] Laboratory of Mechanical Engineering, National Engineering School of Monastir, University of Monastir, Tunisia

[3] Laboratory of Mechanics of Sousse, National Engineering School of Sousse, University of Sousse, Tunisia

[4]Département de Génie Mécanique et systèmes complexes, Institut Pprime, University of Poitiers, France

Abstract

This work denotes an insight into compliant multibody systems synthesis. In contrast with classical synthesis approaches, the flexible behavior of the mechanisms' different bodies is taken into account. A set of responses, such as drawn path, velocity, acceleration in addition to flexible bodies' axial displacement have been combined into the same cost function. Both flexible slider-crank and four-bar mechanisms have been considered as illustrative examples. The design variables subsume dimensional, i.e. the flexible links' length and the material characteristics' such as the Young modulus and material density. Seven optimization techniques have been implemented, mainly, the Biogeography Based Algorithm (BBA), Cultural Algorithm (CA), Firefly Algorithm (FA), Harmonic Search (HS), Invasive Weed (IW), Shuffled Complex Evolution (SC), and the Shuffled Frog (SF). The combined synthesis approach has been investigated beside single based response synthesis. It's been confirmed that involving a single response for a compliant mechanism couldn't vow high accuracy and random responses are witnessed for the mechanism's components non-involved in the synthesis. Whereas, the combined synthesis did joy optimizing the responses of all the mechanism bodies' simultaneously.

Keywords: Flexible multibody system, Optimization, Mechanism synthesis, Metaheuristics, motion and path generation.

1. Introduction

The design for a mechanism will ultimately take cues from the path or motion it is intended to draw. Therefore, the workspace will dictate limits on mechanism size as well as constraints. Accuracy has been a key metric for mechanisms performance assessment. Thus, a target response, whether a given path, motion, or function is drawn thanks to the mechanism end-effector. However, with high velocity, acceleration, and weight capacity to convey, the classical synthesis approach doesn't meet anymore industrial and technical requirements. Due to inevitable manufacturing imperfections, often non-considered throughout the classic synthesis approach, such as clearance in the mechanical joints, wear, friction, and flexible behavior of the mechanism's components, a large discrepancy has been noticed for the real besides expected responses. These imperfections engender a large disturbed response witnessed namely on the end-effector response[1]. In addition, the synthesis has been focused always on a single

response. Consequently, the designer is facing a difficult decision in most of the cases, namely for complicated mechanical devices, to satisfy a single response and completely dismissing the other ones. Multibody systems synthesis has been often treated in three paradigms, path, motion and function generation.

The optimal design variables for a given mechanism have been commonly optimized based on its end-effector path. The four-bar mechanism synthesis based on its coupler drawn path has been of interest for Bai and Angeles [2]. The synthesis problem has been solved by means of algebraic iterative converging to a single solution. Han et al [3] have treated a rigid four-bar topology optimization in order to satisfy the desired path using the Fourier descriptors. Shao et al [4] have proposed a robotized gain rehabilitation for home healthcare device based on two different transformation mechanisms, a slider-crank, and seven-bar. The genetic algorithm has been deployed for the synthesis problem resolution subject to constraints. Ebrahimi and Payvandy [5] have focused on a comparative study for a set of meta-heuristics optimization techniques namely the genetic algorithm, differential evolution, and the imperialist competitive algorithm. Parlaktaş et al [6] have treated a geared four-bar mechanism within collinear input and output shafts. Hadizadeh Kafash and Nahvi [7] have studied a four-bar mechanism synthesis based on its generated path. By means of the circular proximity function, the error separating the obtained and target paths for each one of its constitutive points has been evaluated. An adjustable four-bar mechanism for filleted rectangular path generation has been studied in Ganesan and Sekar [8] work. Based on the balanced positions for different configurations, the optimal architecture of a rigid four-bar mechanism has been defined by means of analytical optimization in [9]. Hernández et al [10] have focused on rigid body four-bar mechanism synthesis using the gradient-based method. Different situations have been investigated and assessed in order to ensure avoiding any eventual singularity. A partially compliant four-bar mechanism has been of interest in [11]. Links' lengths and stiffness have been optimized using the derivative formulation. Bai [12] has formulated the coupler algebraic equation for a spherical four-bar mechanism synthesis. The path synthesis of the mechanism has been carried out for different scenarios to exhibit the proposed approachability to solve similar problems. Xu et al [13] have studied a kinematic synthesis for a partially compliant four-bar mechanism. In addition to the four-rigid links, a flexible beam replaced the revolute joint relating the connector to the follower. Six design variables have been optimized in order to satisfy a desired path for the connector mid-point. The non-sorting genetic algorithm has been deployed to solve the multi-objective optimization problem. Yildiz [14] has focused on a trunk lid mechanism for a sedan car. Modelling the lid system by means of two parallel four-bar mechanisms, the necessary hand force to acting on the lid has been minimized. To do so, the two mechanisms links' lengths have been optimized with several optimization techniques such as PSO, DE and GA. Olinski et al [15] have modelled a knee joint using a rigid four-bar mechanism. Based on the real walker movement, the mechanism links' parameters have been optimised subject to the follower prescribed path. Numerical simulations have been carried-out under MSC ADAMS software for validation.

Due to its complexity, motion generation synthesis has been treated with less interest. Jean-Collard et al. [16] have studied a motion generation synthesis for four-bar and six-bar extensible link mechanisms. The extensible links have been modelled by means of springs. Two optimization strategies have been investigated. The first one relies on minimizing each variable dimension deviation along one cycle of the mechanism motion. Whereas all the parameters have been involved simultaneously for the second approach. A multi-phase motion generation synthesis for the four-bar mechanism has been the interest of Venkataramanujam and Larochelle [17]. Lin and Hsiao [18] have proposed a new motion generation approach involving the transformation of pole maps. Two illustrative examples have been considered, a belt

mechanism within three target positions, and a geared linkage mechanism for four-position. The optimization of the motion and transmission indices for a Delta parallel robot has been the focus Brinker et al [19]. Five design variables have been considered for the optimization problem under workspace and singularity constraints. The motion generation synthesis for a planar four-bar mechanism, using wavelet series theory, has been the aim of Sun et al [20].

A handful of works have been devoted to the function generation synthesis. Alizade and Gezgin [21] have treated a spatial spherical four-bar mechanism optimization. By means of six independent design variables, quaternion algebra has been deployed with the Chebychev approximation to provide optimal design variables. It has been proven that the Chebychev approximation error has the best performance besides the interpolation approximation, least-square approximation, and fitting error extremums. Wu et al [22] have dealt with a fully analytical synthesis for a rigid four-bar mechanism. Using a polynomial approximation of the end-point coordinates, the equation of the coupler curve has been defined.

Metaheuristic's techniques are the most prominent to solve mechanism synthesis and optimization problems. They have been used in tremendous applications focusing on design and optimization such as path and motion planning [23], active and passive self-reconfigurable robot [24], adaptive wheel shape,[25], parallel manipulator knee-amputated rehabilitation mechanism, multi-point haptic device [26], and Parallelogram system [27].

The difference between real manufactured mechanisms' responses and simulation results has been a real challenge for designers. This is due to the avoidance of the mechanism's real behavior during simulation, i.e. flexible behavior of its bodies. It can be inferred throughout previous works[28–32], that mechanisms synthesis has been limited only to rigid mechanisms subsuming perfect joints. Similar assumptions are a real root of inaccuracy. Moreover, mechanism synthesis has been limited only to a single target response. To circumvent these limitations, a new approach for compliant multibody systems synthesis is discussed in this work. Considering the flexible behavior of the mechanism, synthesis has been based on several responses simultaneously such as, the end-effector path, velocity, acceleration as well as the flexible bodies mid-points axial displacements. Two benchmark mechanisms are of scope, a flexible slider-crank and four-bar. Six design variables have been optimized for the flexible slider-crank mechanism, whereas twelve parameters have been targeted for the four-bar. The main contributions of this work are, (1) compliant mechanisms synthesis considering the components flexible behavior, (2) establish both the dimensional and material characteristic synthesis, (3) satisfy all the mechanism responses simultaneously instead of focusing on a single one.

The paper is structured as follows, section 2 deals with the motion equations of both the flexible slider-crank and four-bar mechanisms. The synthesis and optimization problem has been detailed in section 3. The different optimization algorithms used in this paper are discussed in section 4. Section 5 focuses on the main obtained results. The principal conclusions drawn in the work are summarized in section 6.

2. Dynamics of compliant mechanism

The resolution approach for differential-algebraic equations of multibody systems has been the interest in several works [33–36]. Another approach, namely for flexibles multibody systems, based on the dyad finite elements can be used [37]. Following the same resolution method, the motion equations for the flexible mechanisms of scope in this work have been established.

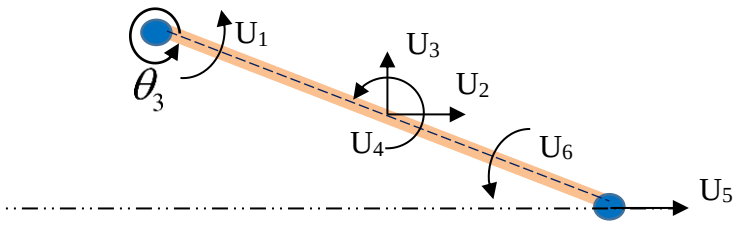

Figure 1 : The flexible beam general coordinates

The six general coordinates describing a flexible beam are detailed in Figure 1 constituted of two elements. Figure 2 depicts the six general coordinates $u_1, u_2, u_3, u_4, u_5, u_6$, for the flexible beam.

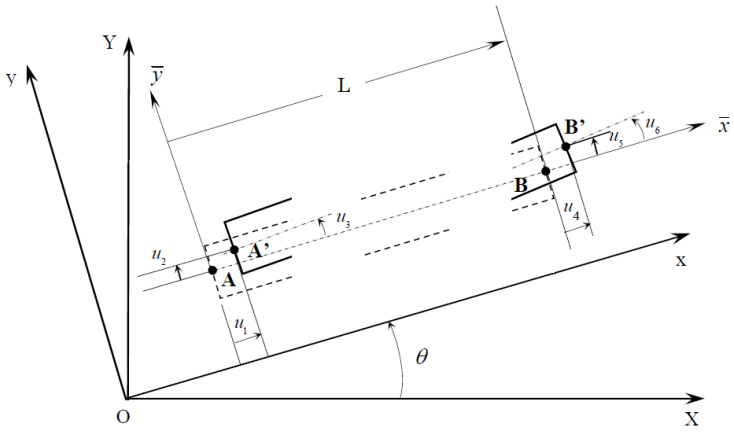

Figure 2: The flexible beam in both rigid and deformed configurations

The absolute acceleration for a beam element can be written as shown in Eq1:

$$\ddot{\mathbf{u}}_{\mathbf{a}} = \ddot{\mathbf{u}}_{\mathbf{r}} + \ddot{\mathbf{u}} + \mathbf{a}_{\mathbf{n}} + \mathbf{a}_{\mathbf{c}} + \mathbf{a}_{\mathbf{t}} \tag{1}$$

Wherein, accelerations are respectively, the rigid element acceleration, the generalized relative acceleration, normal acceleration, Coriolis, and tangential accelerations. The explicit forms for the rigid and absolute accelerations are written in Eq 2 as:

$$\{\ddot{u}_{ri}\} = \begin{Bmatrix} \ddot{x}_A \\ \ddot{y}_A \\ \ddot{\theta}_A \\ \ddot{x}_B \\ \ddot{y}_B \\ \ddot{\theta}_B \end{Bmatrix} \quad \{\ddot{u}_{ai}\} = \begin{Bmatrix} \ddot{x}_{A'} \\ \ddot{y}_{A'} \\ \ddot{\theta}_{A'} \\ \ddot{x}_{B'} \\ \ddot{y}_{B'} \\ \ddot{\theta}_{B'} \end{Bmatrix} \quad i = 1,...,6. \tag{2}$$

In this work, only two components of the Eq 1 are considered, the rigid element acceleration and the generalized relative acceleration. The normal, Coriolis and tangential accelerations are often neglected because the flexible beam is considered under the assumption of low perturbation [38]. Consequently, the new equation for the beam element acceleration yields:

$$\ddot{u}_a = \ddot{u}_r + \ddot{u} \tag{3}$$

The axial displacement taking place along the x-axis for the flexible beam is:

$$v(\bar{x},t) = \phi_1(\bar{x})u_1(t) + \phi_4(\bar{x})u_4(t) \tag{4}$$

The y-axis transversal displacement is written in equation 5 as:

$$w(\bar{x},t) = \phi_2(\bar{x})u_2(t) + \phi_3(\bar{x})u_3(t) + \phi_5(\bar{x})u_5(t) + \phi_6(\bar{x})u_6(t) \tag{5}$$

The following terms $u_1, u_2, u_3, u_4, u_5, u_6$ describe the local frame general coordinate's displacement.

The explicit forms for the shape functions are:

$$\phi_1(\bar{\mathbf{x}}) = 1 - \frac{\bar{\mathbf{x}}}{L}; \qquad \phi_4(\bar{\mathbf{x}}) = \frac{\bar{\mathbf{x}}}{L} \qquad \phi_2(\bar{x}) = 3\left(\frac{L-\bar{x}}{L}\right)^2 - 2\left(\frac{L-\bar{x}}{L}\right)^3; \qquad \phi_3(\bar{x}) = \bar{x}\left(\frac{L-\bar{x}}{L}\right)^2;$$

$$\phi_5(\bar{x}) = 3\left(\frac{\bar{x}}{L}\right)^2 - 2\left(\frac{\bar{x}}{L}\right)^3; \phi_6(\bar{x}) = -L(L-\bar{x})\left(\frac{\bar{x}}{L}\right)^2$$

Consequently, the motion equation, based on the Lagrange principle for a flexible beam, yields:

$$\frac{d}{dt}\left(\frac{\partial T}{\partial \dot{u}_i}\right) - \frac{\partial T}{\partial u_i} + \frac{\partial U}{\partial u_i} = \bar{Q}_i \tag{6}$$

Where T, U and $\bar{Q}_i$ are respectively the kinetic energy, the deformation energy, and the external forces applied to the beam element.

Consequently, the kinetic energy matrix form can be expressed as:

$$T = \frac{1}{2}\dot{\mathbf{u}}^T \bar{\mathbf{m}} \dot{\mathbf{u}} \tag{7}$$

The reduced matrix formulation for the deformation energy yields:

$$U = \frac{1}{2}\mathbf{u}^T \bar{\mathbf{k}} \mathbf{u} \tag{8}$$

The global motion equation relative to a flexible mechanism relying on the dyad finite element method, considering the flexible beam(s) structural damping, yields:

$$M\ddot{U} + C\dot{U} + KU = -M\ddot{U}_r \tag{9}$$

Wherein *M* and *K*, are respectively the mass and stiffness. The rigid beam represents the right side of the motion equation wherein the explicit form written in eq (10) as:

$$\ddot{U}_r = \begin{Bmatrix} \ddot{U}_{r1} \\ \ddot{U}_{r2} \\ \ddot{U}_{r3} \\ \ddot{U}_{r4} \\ \ddot{U}_{r5} \\ \ddot{U}_{r6} \end{Bmatrix} = \begin{Bmatrix} \ddot{\theta}_3 \\ -L_2\dot{\theta}_2\cos\theta_2 - \frac{L_3}{2}(\dot{\theta}_3^2\lambda + \ddot{\theta}_3\mu) \\ -L_2\dot{\theta}_2\cos\theta_2 + \frac{L_3}{2}(\ddot{\theta}_3^2\lambda - \dot{\theta}_3^2\mu) \\ \ddot{\theta}_3 \\ -L_2\dot{\theta}_2\cos\theta_2 - L_3(\ddot{\theta}_3\mu + \dot{\theta}_3^2\lambda) \\ \ddot{\theta}_3 \end{Bmatrix} \quad (10)$$

Following [38], the damping matrix is expressed as:

$$C_k = 2\zeta_k\omega_k\theta_t\theta_k^T \quad (11)$$

Where, $\theta_k = M\phi_k$, ζ_k is the damping coefficient, ω_k is the k^{th} eigenfrequency, ϕ_k is the k^{th} eigenmode.

Based on the selected eigenmodes numbers, *n*, the damping matrix yields:

$$C = \sum_{k=1}^{n} C_k \quad (12)$$

Equation 13, allows solving the free vibration systems as a first step. Consequently, the eigenvalues for the system can be defined. The next step for the resolution will be to solve the motion equation for the whole system.

$$K\phi_n = \omega_n^2 M\phi_k \quad (13)$$

Where ϕ_n and ω_n^2 are respectively the eigenmode and the eigenfrequency.

The modal coordinates should be used as written in eq 14:

$$\begin{aligned} U &= \Phi\eta \\ \dot{U} &= \Phi\dot{\eta} \\ \ddot{U} &= \Phi\ddot{\eta} \end{aligned} \quad (14)$$

Where Φ and η are respectively the modal matrix and the modal amplitude.

Finally, equation 9 yields:

$$\Phi^T M\Phi\ddot{\eta} + \Phi^T C\Phi\dot{\eta} + \Phi^T K\Phi\eta = -\Phi^T M\ddot{U}_r \quad (15)$$

The general motion equation for each eigenmode yields:

$$M_{ii}^{\eta}\ddot{\eta}_i(t) + C_{ii}^{\eta}\dot{\eta}_i(t) + K_{ii}^{\eta}\eta_i(t) = N_i(t) \quad (16)$$

Where

$$M^{\eta} = \Phi^{T} M \Phi$$
$$C^{\eta} = \Phi^{T} C \Phi$$
$$K^{\eta} = \Phi^{T} K \Phi$$
$$N = -\Phi^{T} M \ddot{U}_{r}$$

The characteristic parameters for the target mechanisms used to generate the target responses, depicted in Figure 3, are detailed in Table 1.

Table 1: The slider-crank and four-bar mechanism parameters

The crank angular velocity (θ_2)	**Slider-crank**	26.18 rd/ sec
	Four-bar	
The crank length (l_2)	**Slider-crank**	50 mm
	Four-bar	100 mm
The flexible connecting-rod/coupler length (l_3)	**Slider-crank**	350 mm
	Four-bar	250 mm
The flexible follower length (l_4)	**Slider-crank**	
	Four-bar	250 mm
The frame length (l_1)	**Slider-crank**	-
	Four-bar	285 mm
The flexible connecting rod/connector/follower density	**Slider-crank**	2660 kg/m^3
	Four-bar	
The flexible connecting rod/connector/follower Young modulus	**Slider-crank**	71000 MPa
	Four-bar	
The flexible connecting rod/connector/follower cross-section	**Slider-crank**	0.36 10^{-4} m²
	Four-bar	
The crank cross-section	**Slider-crank**	4.68 10^{-4} m²
	Four-bar	
The slider mass	**Slider-crank**	0.245 kg
	Four-bar	-

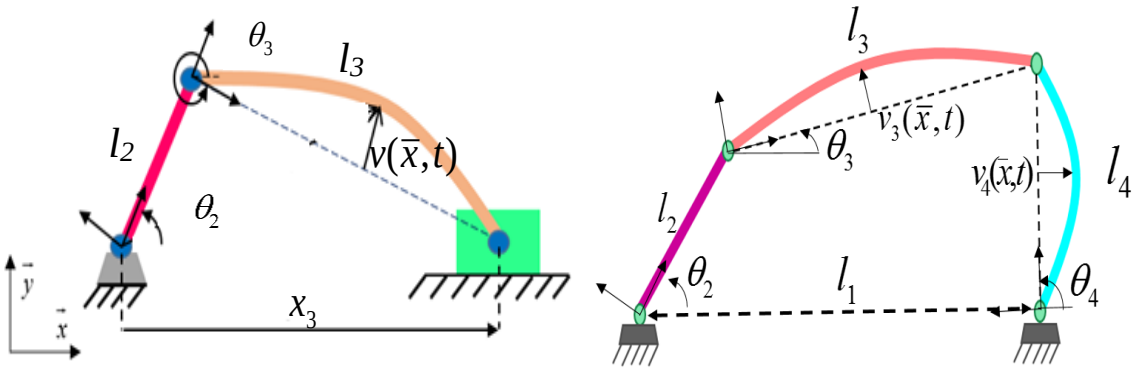

(a) (b)

Figure 3: The flexible mechanisms; (a) slider-crank, (b) four-bar

3. The synthesis and optimization problem formulation

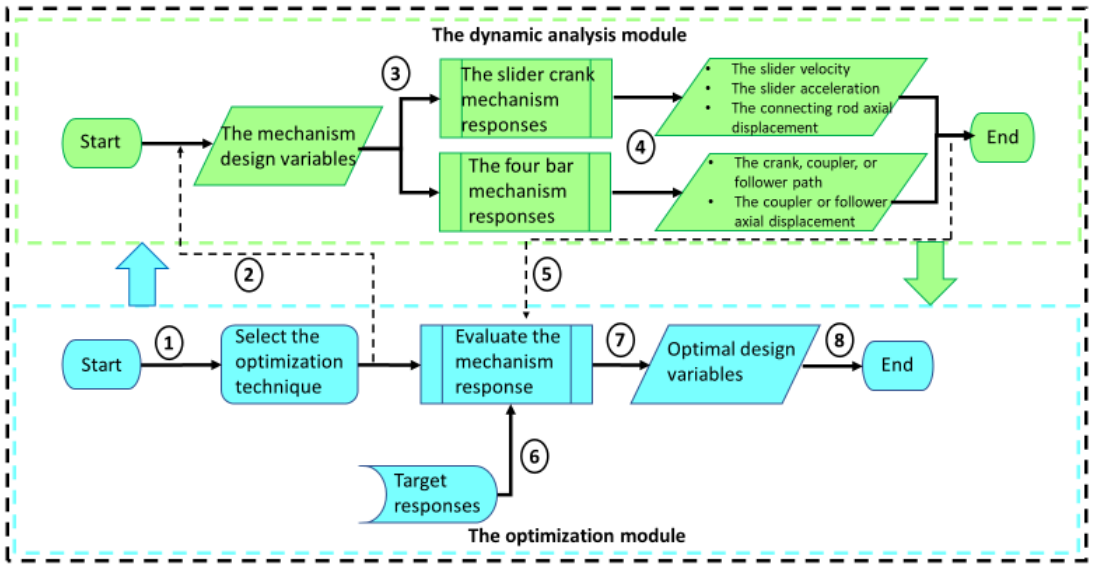

Figure 4: The interaction between optimization module and dynamic analysis module for compliant multibody systems synthesis

The general optimization approach discussed in this work is divided into two major parts:

- The dynamic modeling (detailed in section 2).
- The optimization and synthesis**.**

The aforementioned parts are connected in order to exchange whether the design variables or dynamic responses as exhibited in Figure 4. The first step of the proposed synthesis approach consists of selecting the optimization technique and generating the random initial population from the defined search intervals subject to the required constraints (arrow 1). Then, the generated initial population is sent to the dynamic model for the flexible mechanism (arrow 2) in order to simulate their responses (arrow 3). Subsequently, the obtained dynamic responses are stored (arrow 4) and sent back to the optimization module (arrow 5). At this level, the

performance of each design variables response' is evaluated by means of the cost function. As shown in arrow 6, the target responses, obtained by means of mechanisms exhibited in Figure 3, are already defined by the user and given as input. Two scenarios are possible afterward this step, if the defined number of iteration or the error threshold is reached, the algorithm will follow the arrow 7 and 8 to be ended. Else, it will start again and the same process from arrow 1 to arrow 7 will take place.

Mechanisms' synthesis has been formulated as an optimization problem. Thus, acting on several design parameters, usually dimension and geometric, the error between target and obtained paths is reduced [39,40]**.** In sharp contrast with the real case, mechanisms studied have been considered under the assumption of rigid bodies. Conversely, several experimental works [37,41] confirmed that the mechanism's bodies behave as flexible in real applications. Consequently, the end effector response is different from the expected one. To circumvent this limitation, the flexible behavior of the mechanism's components is considered in this work. Moreover, a set of responses have been considered simultaneously for the synthesis process instead of focusing only on a single path or motion completely dismissing the other mechanism's components responses. To do so, a generic core cost function is created to assess all types of responses, whether velocity, acceleration, or axial displacement providing a dimensionless scalable metric. The core cost function is implemented in a way to deal with different mechanism synthesis, such as slider-crank and four-bar. In order to be able to evaluate the obtained responses beside a reference one and due to the lack of reference responses for compliant mechanisms synthesis in the literature, the authors have chosen some given responses based on already known mechanisms as detailed previously in Table 1 and Figure 3. Notwithstanding, these target responses could be changed depending on the desired response to fulfill. The formulated cost functions are designed to evaluate any response type, it could be even based on some given point coordinates. The error evaluated in each instant is divided by the absolute value of the minimum and maximum values obtained in the response curve as witnessed in Figure 5 providing a dimensionless scalar.

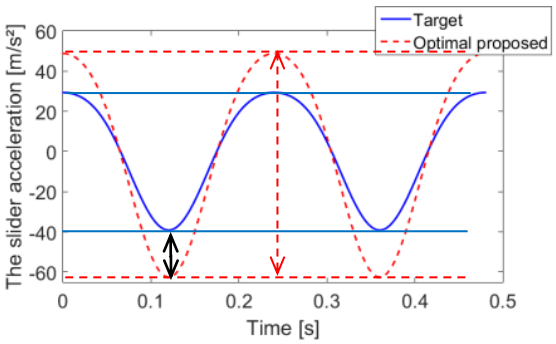

Figure 5 The error evaluation

3.1 The flexible slider-crank mechanism synthesis

The slider-crank mechanism synthesis has been carried out based on different response types, the slider, velocity, acceleration, and the flexible connecting-rod mid-point axial displacement. These responses have been combined to conclude a trade-off between all of them. Based on the core cost function satisfying criterion discussed above, the error between the target and obtained responses are evaluated by means of eq 17:

$$fitness = Minimize(f(\mathrm{R})) \tag{17}$$

Where: $f(\mathrm{R}) = \sqrt{\frac{1}{N}\sum_{i=1}^{N}\left[\frac{R_i(\mathbf{X}) - R_i^*}{Max(\mathrm{R}_i(\mathbf{X})) - Min(\mathrm{R}_i(\mathbf{X}))}\right]^2}$ (18)

$$
\begin{aligned}
&Subject\ to:\\
&l_2\cos\theta_2 + l_3\cos\theta_3 - x_3 = 0\\
&l_2\sin\theta_2 + l_3\sin\theta_3 = 0\\
&L_{b2} \le l_2 \le U_{b2}\\
&L_{b3} \le l_3 \le U_{b3}\\
&l_2 < l_3\\
&L_{b4} \le \rho \le U_{b4}\\
&L_{b5} \le E \le U_{b5}\\
&L_{b6} \le a \le U_{b6}\\
&L_{b7} \le h \le U_{b7}
\end{aligned}
\qquad (19)
$$

Wherein, L_{bi}, U_{bi} represent respectively the upper and lower bound for the search interval. The design variable vector subsumes the following variables, $\mathbf{X} = [l_2 \quad l_3 \quad \rho \quad E \quad h \quad a]$ respectively for the crank length, connecting-rod's length, density, Young modulus, and the high and width. The parameter $R_i(\mathbf{X})$ represents the mechanism given response using the design variable vector whereas R_i^* represents the target response defined by the user as depicted by arrow 6 in Figure 4. The subscript *i* for both the generated and target responses is related to the number of prescribed points (N) equal to 121 for an average of an acquisition point each 0.04 sec along 0.48 sec. This simulation time covers two crank revolutions.

Substituting the letter R in the core function (Eq 18) yields to equations 20, 21 and 22 dealing respectively with the acceleration error (*f(A)*), velocity error (*f(V)*) and axial displacement error (*f(D)*) beside the target responses.

$$f(\mathrm{A}) = \sqrt{\frac{1}{N}\sum_{i=1}^{N}\left[\frac{A_i(\mathbf{X}) - A_i^*}{Max(\mathrm{A}_i(\mathbf{X})) - Min(\mathrm{A}_i(\mathbf{X}))}\right]^2} \qquad (20)$$

$$f(\mathrm{V}) = \sqrt{\frac{1}{N}\sum_{i=1}^{N}\left[\frac{V_i(\mathbf{X}) - V_i^*}{Max(\mathrm{V}_i(\mathbf{X})) - Min(\mathrm{V}_i(\mathbf{X}))}\right]^2} \qquad (21)$$

$$f(\mathrm{D}) = \sqrt{\frac{1}{N}\sum_{i=1}^{N}\left[\frac{D_i(\mathbf{X}) - D_i^*}{Max(\mathrm{D}_i(\mathbf{X})) - Min(\mathrm{D}_i(\mathbf{X}))}\right]^2} \qquad (22)$$

For the combined optimization, the three mechanism responses should be involved simultaneously in the fitness function. A weight coefficient has been attributed to each response based on a parametric study carried out in [42] as detailed in eq23.

$$f(A,V,D) = \alpha f(\mathrm{D}) + \beta f(\mathrm{V}) + \gamma f(\mathrm{A})$$
$$= \alpha \sqrt{\frac{1}{N}\sum_{i=1}^{N}\left[\frac{D_i(X) - D_i^*}{Max(\mathrm{D}(\mathbf{X})) - Min(\mathrm{D}(\mathbf{X}))}\right]^2} + \beta \sqrt{\frac{1}{N}\sum_{i=1}^{N}\left[\frac{V_i(\mathbf{X}) - V_i^*}{Max(\mathrm{V}(\mathbf{X})) - Min(\mathrm{V}(\mathbf{X}))}\right]^2} \quad (23)$$
$$+ \gamma \sqrt{\frac{1}{N}\sum_{i=1}^{N}\left[\frac{A_i(\mathbf{X}) - A_i^*}{Max(\mathrm{A}(\mathbf{X})) - Min(\mathrm{A}(\mathbf{X}))}\right]^2}$$

$$\alpha = 0.4, \beta = \gamma = 0.3 \quad (24)$$

3.2 The flexible four-bar mechanism synthesis

Since the four-bar mechanism subsumes two flexible bodies, its synthesis should be treated differently. Usually, for rigid four-bar mechanisms, the main focus is devoted to a single response, the coupler path [28–32]. However, when the flexible behavior of the mechanism components is considered, this approach couldn't be accurate neither vouch that the mechanisms' components satisfy the desired drawn paths. Consequently, the crank, flexible coupler, as well as flexible follower midpoint drawn paths, are considered. In addition, to keep the axial displacement during the synthesis process in acceptable thresholds, both axial displacements of the coupler and follower have been involved toward the mechanism synthesis. By means of the proposed core cost function in Eq 18, combining all the five responses is possible providing a normalized and dimensionless error.

Errors following the X and Y axis for prescribed paths of the crank, coupler, and follower beside the target ones, as well as axial displacements for the coupler and follower, have been assessed. Errors have been measured among 121 points of the drawn responses. The design variable vector is written as follow, $X = [l_1 \quad l_2 \quad l_3 \quad l_4 \quad E_3 \quad \rho_3 \quad h_3 \quad a_3 \quad E_4 \quad \rho_4 \quad h_4 \quad a_4]$. The cost function is formulated following Eq (25):

$$f = \sqrt{\frac{1}{N}\sum_{i=1}^{N}\left[\left(\frac{x_{cri}(X) - x_{cri}^*(X)}{Max(x_{cri}(X)) - Min(x_{cri}(X))}\right)^2 + \left(\frac{y_{cri}(X) - y_{cri}^*(X)}{Max(y_{cri}(X)) - Min(y_{cri}(X))}\right)^2\right]}$$
$$+ \sqrt{\frac{1}{N}\sum_{i=1}^{N}\left[\left(\frac{x_{coi}(X) - x_{coi}^*(X)}{Max(x_{coi}(X)) - Min(x_{coi}(X))}\right)^2 + \left(\frac{y_{coi}(X) - y_{coi}^*(X)}{Max(y_{coi}(X)) - Min(y_{coi}(X))}\right)^2\right]}$$
$$+ \sqrt{\frac{1}{N}\sum_{i=1}^{N}\left[\left(\frac{x_{foi}(X) - x_{foi}^*(X)}{Max(x_{foi}(X)) - Min(x_{foi}(X))}\right)^2 + \left(\frac{y_{foi}(X) - y_{foi}^*(X)}{Max(y_{foi}(X)) - Min(y_{foi}(X))}\right)^2\right]} \quad (25)$$
$$+ \sqrt{\frac{1}{N}\sum_{i=1}^{N}\left[\frac{D_{coxi}(X) - D_{coxi}^*(\mathrm{X})}{Max(D_{coxi}(\mathbf{X})) - Min(D_{coxi}(\mathbf{X}))}\right]^2} + \sqrt{\frac{1}{N}\sum_{i=1}^{N}\left[\frac{D_{foxi}(\mathbf{X}) - D_{foxi}^*(X)}{Max(D_{foxi}(\mathbf{X})) - Min(D_{foxi}(\mathbf{X}))}\right]^2}$$

$$
\begin{aligned}
&\textit{Subject to}: \\
&l_2 + l_4 < l_1 + l_3 \\
&l_2 + l_3 < l_1 + l_4 \\
&l_1 + l_2 < l_3 + l_4 \\
&L_{b1} \le l_1 \le U_{b1} \\
&L_{b2} \le l_2 \le U_{b2} \\
&L_{b3} \le l_3 \le U_{b3} \\
&L_{b4} \le l_4 \le U_{b4} \\
&L_{b5} \le \rho_3 \le U_{b5} \\
&L_{b6} \le E_3 \le U_{b6} \\
&L_{b7} \le a_3 \le U_{b7} \\
&L_{b8} \le h_3 \le U_{b8} \\
&L_{b9} \le \rho_4 \le U_{b9} \\
&L_{b10} \le E_4 \le U_{b10} \\
&L_{b11} \le a_4 \le U_{b11} \\
&L_{b12} \le h_4 \le U_{b12}
\end{aligned}
\tag{26}
$$

Where, l_1 is the frame length, l_2 is the crank length, l_3 is the flexible coupler length, and l_4 is the flexible follower length.E_3, E_4,a_3,a_4,h_3,h_4,ρ_3 *and* ρ_4 are the young modulus, width, height and material density for the flexible coupler and follower respectively. The parameters x_{foi} y_{foi} x_{coi} y_{coi} x_{cri} y_{cri} represent the coordinates along x and y-axis respectively for the follower, coupler, and crank midpoints. Whereas, all variables labeled with a star such as x^*_{foi}, y^*_{foi}, x_{coi}, y_{coi}, x^*_{cri} and y^*_{cri} characterize the target response coordinates respectively for the follower, coupler and crank. D_{cox} , D_{fox} , are respectively the coupler and follower axial displacements, meanwhile, D^*_{cox} and D^*_{fox} are the one's relative to the target response.

4. Metaheuristic optimization techniques for the synthesis problem resolution

Regarding its complexity, the meta-heuristics optimization techniques are the most convenient to solve similar synthesis problems. The performance of the different techniques implemented in this work is discussed in order to give some guidelines to the user about the accuracy of each one of them.

Table 2: The slider-crank parameters' search intervals

Parameters	l_2 **(mm)**	l_3 **(mm)**	E **(kPa)**	ρ **(kg/m^3)**	h**(mm)**	a **(mm)**
Search interval $[L_b, U_b]$	[20;80]	[200;500]	[6.5 10^{10} ;7.5 10^{10}]	[2000;3000]	[1;2]	[20;30]

Search intervals for the design variable parameters characterizing the slider-crank mechanism, namely, the crank (l_2), the flexible connecting rod (l_3) lengths, material density (ρ), Young Modulus (E), high (h) and width (a), are summarized in Table 2. Whereas, parameters relative to the four-bar mechanism are detailed in Table 3.

Table 3: The four-bar parameters' search intervals

Parameters	l_1 **(mm)**	l_2 **(mm)**	l_3 **(mm)**	l_4 **(mm)**	E_3 **(kPa)**	ρ_3 **(kg/m^3)**
Search interval	[100;300]	[70;200]	[200;300]	[200;300]	[6.5 10^{10} ;7.5 10^{10}]	[2000;3000]
Parameters	h_3**(mm)**	a_3 **(mm)**	h_4**(mm)**	a_4 **(mm)**	E_4 **(kPa)**	ρ_4 **(kg/m^3)**
Search interval	[1;2]	[20;30]	[1;2]	[20;30]	[6.5 10^{10} ;7.5 10^{10}]	[2000;3000]

Basically, seven optimization techniques are of scope in this work. However, only the Biogeography Based Optimization (BBA), Cultural Algorithm (CA), Firefly Algorithm (FA), Harmonic Search (HS) and Invasive Weed (IW) methods are detailed. For the remaining techniques, readers could refer to the above reference for more details. The pseudo-code for the BBA algorithm implemented along this work is presented in Algorithm 1.

Algorithm 1: Biogeography Based Algorithm pseudo-code [43]

```
Create random habitats
Generate each created habitat response.
Evaluate each created habitat based on the cost function.
Sort the different habitats based on their fitness function scores.
For i=1 to maximum number of iterations
    For i=1 to max number of population size
      For l=1 to number of variables
      Generate a random migration value
        If random migration value <= immigration rate
         Migration process takes place for the l^th components of the design variable vector
          Else migration process doesn't take place.
          End
        Generate a random mutation value
        If random mutation value <= mutation rate
         Mutation process takes place for the l^th components of the design variable vector
          Else mutation process doesn't take place.
          End
      End
     Generate the new population response
    Evaluate the new population fitness
    Keep the next iteration population.
End
```

The second meta-heuristic optimization technique detailed in this work is the cultural optimization [44] wherein the pseudo-code is detailed in Algorithm 2.

Algorithm 2: Cultural Optimization psedo-code [44]

```
Initialization parameters
Initialize culture
Create random solutions
Generate each random solution response
Evaluate each random solution performance based on the fitness function
Sort the different solutions based on their fitness function score
Adjust cultural using selected solutions
For i=1 to maximum iteration number
For i=1 to population size
    for j=1 to variables number
      evaluate cultures influences on each other's
      substitute the old culture with the new influenced one.
    end
Generate the dynamic responses
Evaluate the new solution performance
End
```

Sort the new population based on each solution performance
Adjust culture based on the selected solutions

Inspired by the firefly swarm movement, the firefly algorithm represents the third detailed optimization technique in this work. The pseudo-code for the aforementioned optimization technique is described in Algorithm 3. Complementary information about this technique can be found in [45].

Algorithm 3:Firefly algorithm psedo-code [45]

Generate the initial population responses.

Evaluate and sort the initial pupation particle based on the fitness function.

```
for it=1 to maximum iteration number
    for i=1 to population size
      for j=1 to population size
        if the j^th firefly cost<the i^th firefly cost
            updates the firefly positions
            Generate each new particle response
            Evaluate each new particle performance
        end
      end
   end
merge the new particle with the existent population
sort the whole population and eliminate the weakest particle.
End
```

Based on the music players and musicians during their spectacle and performances, the Harmonic search algorithm is mimicking the improvisation of music players. The pseudo-code of the implemented technique is detailed in Algorithm 4. Curious readers may refer to [46] for further details about the aforementioned technique.

Algorithm 4: Harmony Search [46]

```
Generate the initial population responses.
Evaluate and sort the initial pupation particle based on the fitness function.
for it=1 to maximum iteration number
   for k=1to maximum number of New Harmonies
       Generate randomly new position subject to search interval for each parameter
      for j=1 to Variable size
         Generate a random coefficient from [0,1]
          if rand<= Harmony Memory Consideration Rate
            i=random number from [1, Harmony Memory Size];
            The j^th Parameter of the kth new harmony=the j^th Position of the i^th intial generated harmony;
         end
           Generate a random coefficient from [0,1]
         if rand<= Pitch Adjustment Rate
            Update the j^th Position of the k^th new harmony and Pitch Adjustment
         end
      end
        Generate each new Harmony response
        Evaluate each new Harmony performance
   end
   Merge the new particle with the existent population
   Sort the whole population and eliminate the weakest particle.
```

Inspired by weeds behavior, the Invasive weed algorithm has been created. More details about the used algorithm in this work can be found in [47]. Algorithm 5 depicts the pseudo-code implemented in the present work.

Algorithm 5: Invasive weed [47]

```
Generate a random initial population of weeds
Simulate the dynamic response for each generated weed for the initial population.
Evaluate each weed performance based on the fitness function
for it = 1 to maximum iteration number
    Update the standard deviations
  for i = 1 to population size
       Create random new solutions.
       Remove back new out of swarm particle to the swarm.
       Generate the new weed position dynamic responses.
       Evaluate the performance of the new response based on the fitness function
       Add the new solution to the existent population
   end
  merge, sort, and eliminate the weakest weed position based on the fitness function.
 end
```

Table 4: The used optimization techniques parameters.

	BBA	**CA**	**FO**	**HS**	**IW**	**SC**	**SF**
Maximum number of iterations	250	250	250	250	250	250	250
Initial population size(nPop)	20	20	20	20	20	20	20
Keep rate	0.2	-	-	-	-	-	-
Number of kept habit(nKeep)	KeepRate*nPop	-	-	-	-	-	-
Number of New Habitats	nNew=nPop-nKeep	-	-	-	-	-	-
Mutation propapility	0.1	-	0.2	-	-	-	-
Acceptation ration (pAccept)	-	0.35	-	-	-	-	-
Number of accepted individuals	-	round(pAccept*nPop)	-	-	-	-	-
Light absorption coefficient	-	-	1	-	-	-	-
Attraction Coefficient Base Value	-	-	2	-	-	-	-
Mutation Coefficient Damping Ratio	-	-	0.98	-	-	-	-
New Harmonies	-	-	-	10	-	-	-
Harmony Memory Consideration Rate	-	-	-	0.9	-	-	-
Pitch Adjustment Rate	-	-	-	0.1	-	-	-
Minimum/max Number of Seeds	-	-	-	-	5/10	-	-
Number of Complexes	-	-	-	-	-	2	2
Number of Offsprings	-	-	-	-	-	3	3
Complex Size	-	-	-	-	-	10	10

The different optimization techniques' parameters used along this work are exhibited in Table 4.

5. Results and discussions

Numerical simulation outcomes for the two flexible mechanisms of scope are discussed toward this section. The slider velocity, acceleration, and flexible connecting-rod mid-point axial displacement have been involved for the flexible slider-crank mechanism synthesis. Albeit, the crank, connector, follower mid-points paths joined to the flexible connector and follower axial displacement have been the synthesis responses for the four-bar mechanism.

5.1. The flexible slider-crank mechanism synthesis

5.1.1. The slider velocity synthesis

In this section, the slider velocity has been chosen as a target response through the synthesis process. As summarized in Table 5, different performances are recorded for the optimization algorithms. The cultural algorithm (CA), shuffled complex evolution (SC), and shuffled frog (SF) techniques lie to an absolute zero error (Figure 6). As it can be seen in Figure 7 and Figure 8, respectively for the slider velocity and acceleration, the optimal responses almost overlap the target ones. Nevertheless, a proportional discrepancy to the evaluated error mentioned in Table 5, is witnessed for the other optimization techniques. Even though only the slider velocity is considered for the synthesis process in this section, the slider acceleration meets the target response for the CA, SC, and SF techniques. This is in perfect agreement with Kim work [48]for the first and second-order derivative curves for the mechanism synthesis.

The gap witnessed in Figure 9, for the axial displacement represents a hurdle stemming from the limitation of involving a single response for the synthesis process. Despite the satisfaction of both the slider velocity and acceleration as consequence due to these two responses' dependence, the axial displacement taking place in the connecting-rod midpoint is far away from the desired one for all the involved techniques.

Table 5: The proposed design variables based on the slider velocity synthesis

	l_2(mm)	l_3(mm)	ρ(kg/m^3)	E (kPa)	b(mm)	h(mm)	Error
BBA	49.9860	349.8059	2.5838 10^3	6.8616 10^{10}	20.7854	1.1471	9.7182 10^{-5}
CA	50.0000	350.0000	3.0979 10^3	7.0779 10^{10}	24.4129	1.8094	0
FO	49.9999	350.0007	2.7569 10^3	6.9324 10^{10}	25.4711	1.1419	1.6682 10^{-7}
HO	50.0010	350.0544	2.4059 10^3	7.0424 10^{10}	26.4479	1.6718	7.6991 10^{-6}
IW	50.0115	349.8703	2.1866 10^3	6.9897 10^{10}	30.0000	1.6075	8.3273 10^{-5}
SC	50.0000	350.0000	2.4136 10^3	7.0731 10^{10}	25.5249	1.4070	0
SF	50.0000	350.0000	2.7440 10^3	7.4101 10^{10}	22.6306	1.7233	0

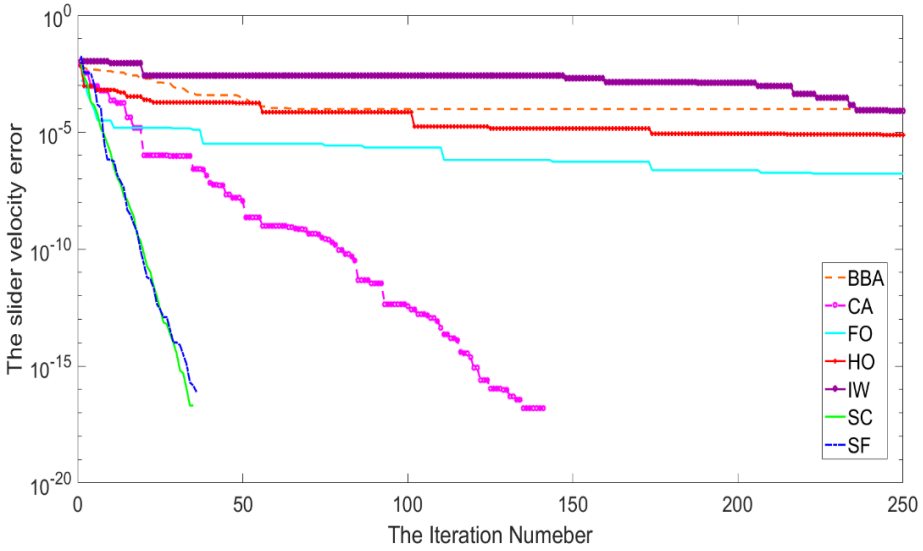

Figure 6: The velocity error evolution

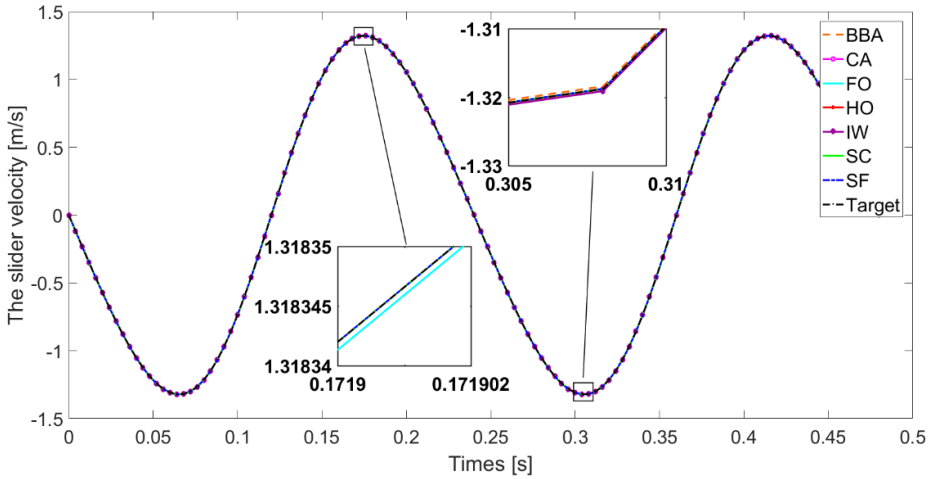

Figure 7: The slider velocity responses based on the slider velocity synthesis

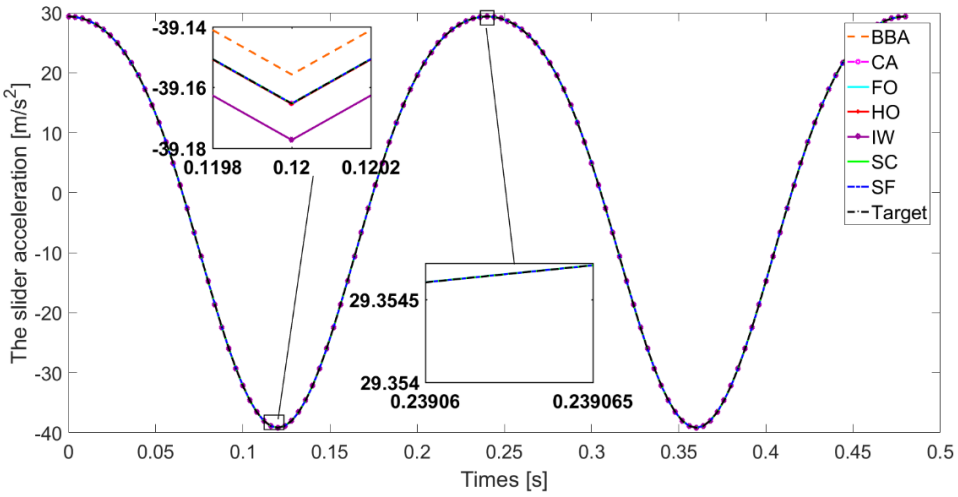

Figure 8: The slider acceleration responses based on the slider velocity synthesis

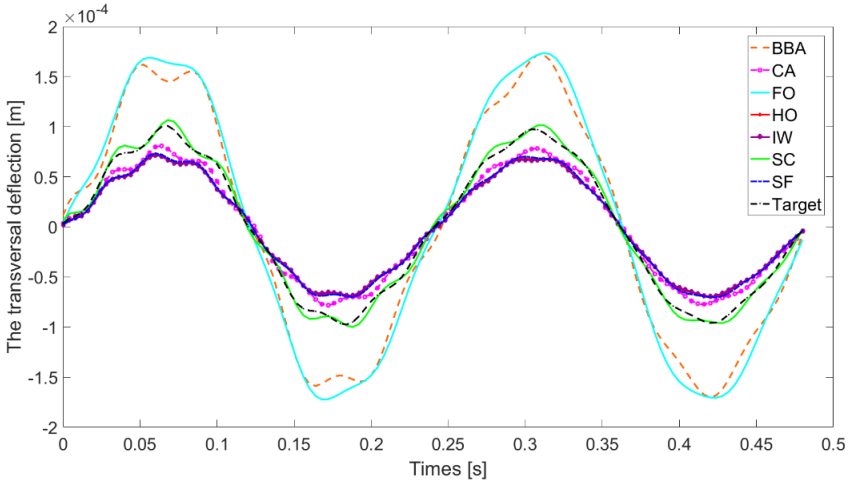

Figure 9: The axial displacement responses based on the slider velocity synthesis

5.1.2. The axial displacement synthesis

To further investigate the results of section 5.1, the mechanism synthesis is carried-out considering the axial displacement of the flexible connecting-rod as a target response. The SC optimization technique is on the lead proposing a design variables solution wherein error worth 1.434810^{-8}. The main obtained results are compiled in Table 6. It can be witnessed in Figure 10 for the error evolution, that this synthesis paradigm represents a burdensome task to fulfill. Figure 11 and Figure 12 respectively for the slider velocity and acceleration responses depict a considerable discrepancy confirming that the axial displacement synthesis satisfies just the involved response in Figure 13. Thus, the optimal design variable responses completely dismiss the slider velocity and acceleration. This phenomenon has been witnessed in section 5.1.1 confirming that solely the involved response for the synthesis is satisfied, whereas, the mechanism's avoided bodies behave randomly. To circumvent this limitation, all the mechanism responses should be involved simultaneously in the same cost function. In what follows, section 5.1.3 addresses utmost care to the combined synthesis of compliant mechanism.

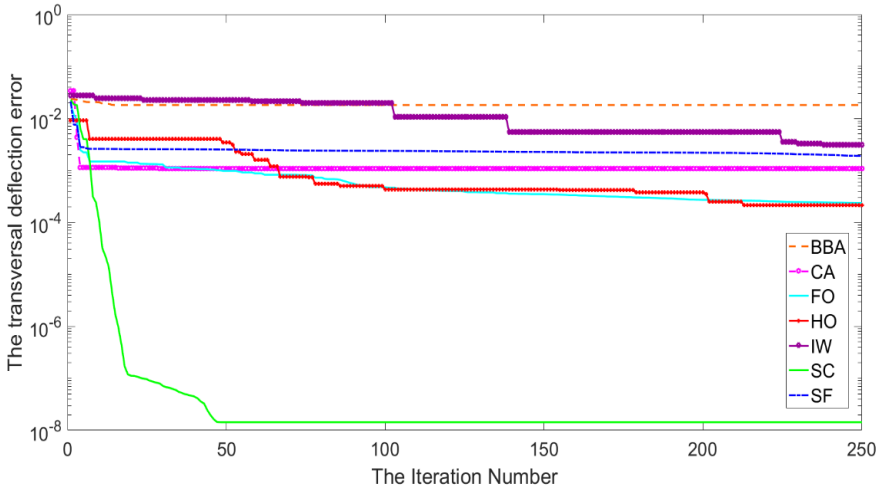

Figure 10: The axial displacement error evolution

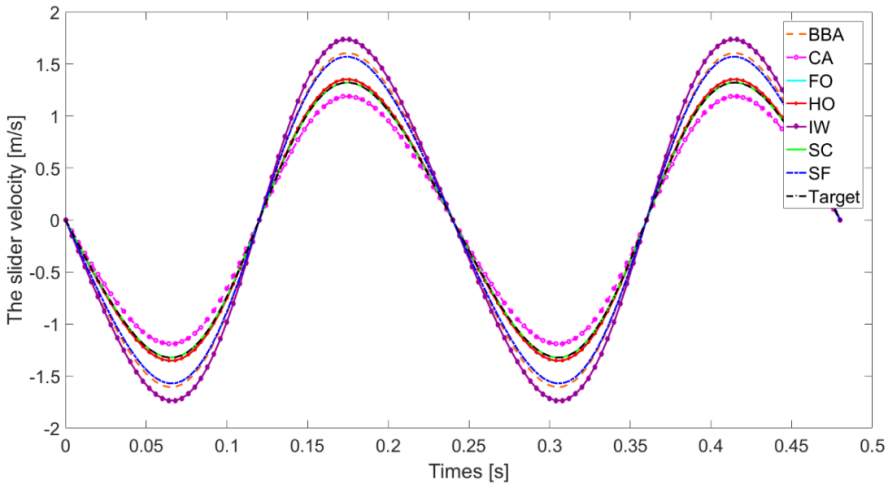

Figure 11: The slider velocity based on the axial displacement synthesis

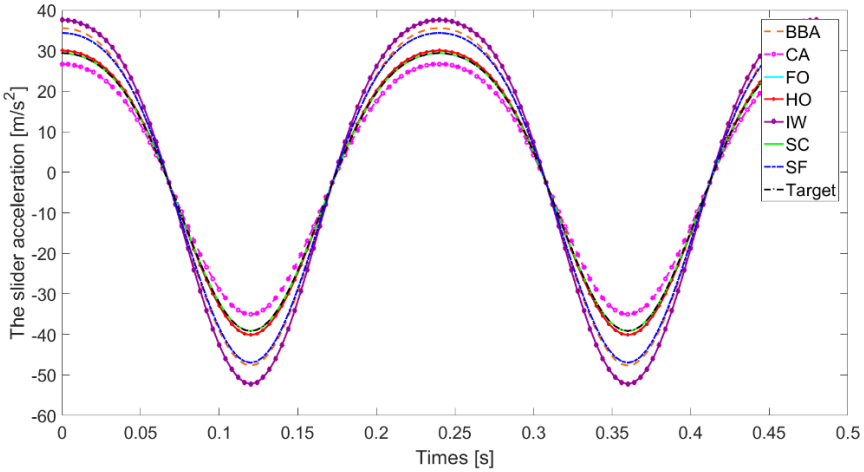

Figure 12: The slider acceleration based on the axial displacement synthesis

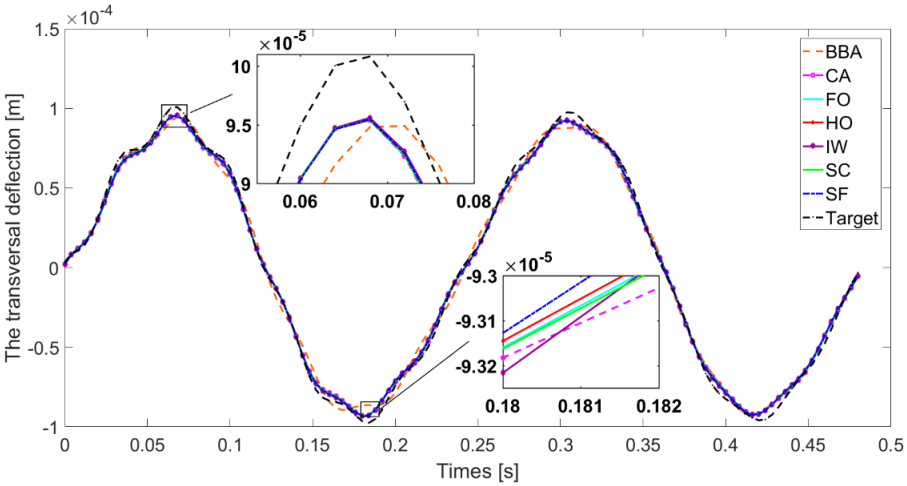

Figure 13: The axial displacement responses based on the axial displacement synthesis

Table 6: The flexible connecting rod mid-point axial displacement optimization results

	l_2(mm)	l_3(mm)	$\rho(kg/m^3)$	E (kPa)	b(mm)	h(mm)	Error
BBA	60.7163	416.9371	$2.2695\ 10^3$	$7.0899\ 10^{10}$	20.0000	1.8558	$1.8062\ 10^{-2}$
CA	45.0594	332.0981	$2.5618\ 10^3$	$7.1128\ 10^{10}$	23.6719	1.3518	$1.0785\ 10^{-3}$
FO	51.2454	354.3549	$2.3474\ 10^3$	$6.7143\ 10^{10}$	30.0000	1.5157	$2.3522\ 10^{-4}$
HO	51.1442	353.9920	$2.8451\ 10^3$	$7.3713\ 10^{10}$	29.8226	1.5895	$2.1497\ 10^{-4}$
IW	65.4826	400.9554	$2.4513\ 10^3$	$6.5838\ 10^{10}$	26.9225	2.0000	$3.0986\ 10^{-3}$
SC	50.0002	350.0007	$2.3860\ 10^3$	$7.0375\ 10^{10}$	24.8891	1.4562	$1.4348\ 10^{-8}$
SF	59.3282	381.5754	$2.6621\ 10^3$	$7.0451\ 10^{10}$	25.2267	1.8260	$1.9014\ 10^{-3}$

5.1.3. The combined error synthesis

Based on the previous assertions in sections 5.1.1 and 5.1.2, it could be inferred that the designer is constrained to whether satisfy the target dynamic responses namely the slider velocity and acceleration or to fit the defined threshold mid-point axial displacement for the flexible connecting rod. Non-withstanding, meeting all the above responses simultaneously is of paramount importance in many industrial applications. To do so, these responses have been involved simultaneously in a combined synthesis. A weight coefficient is given to each response error. The presented results are carried out using the following weight coefficients combination, 0.4, 0.3, and 0.3 respectively for the slider velocity, acceleration and flexible connecting-rod axial displacement errors based on a parametric study [42]. The error evolution plots for the set of implemented optimization techniques are depicted in Figure 14. It can be inferred that both the SF and SC techniques outperform the other optimization techniques for the combined synthesis. The relative error evolution curve for the SF techniques converges in about 60 iterations for an evaluated combined error of $5.9590\ 10^{-9}$.

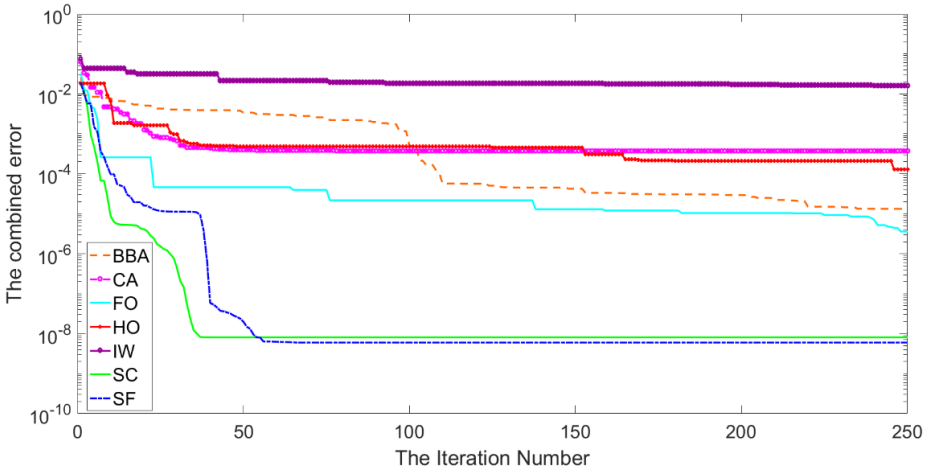

Figure 14: The combined error evolution for the different optimization techniques

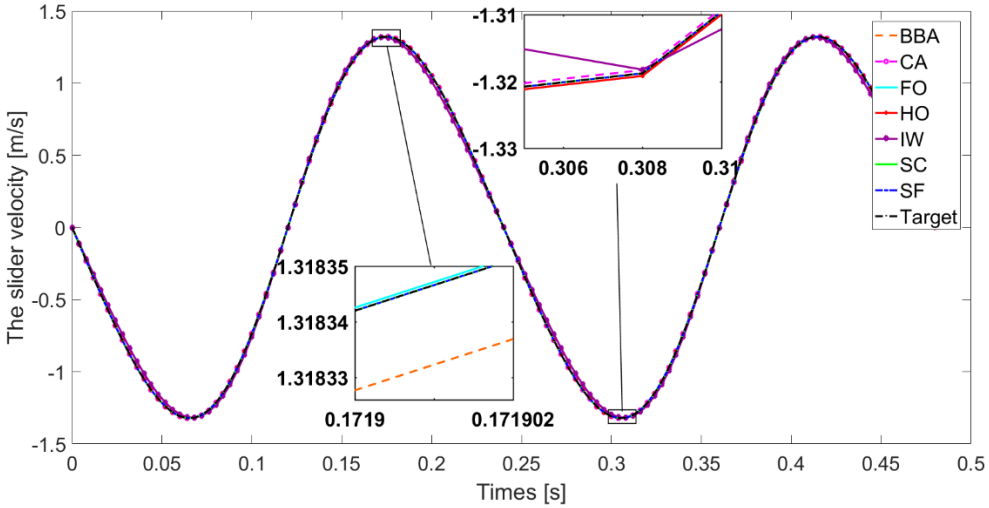

Figure 15: The slider velocity responses based on the combined synthesis

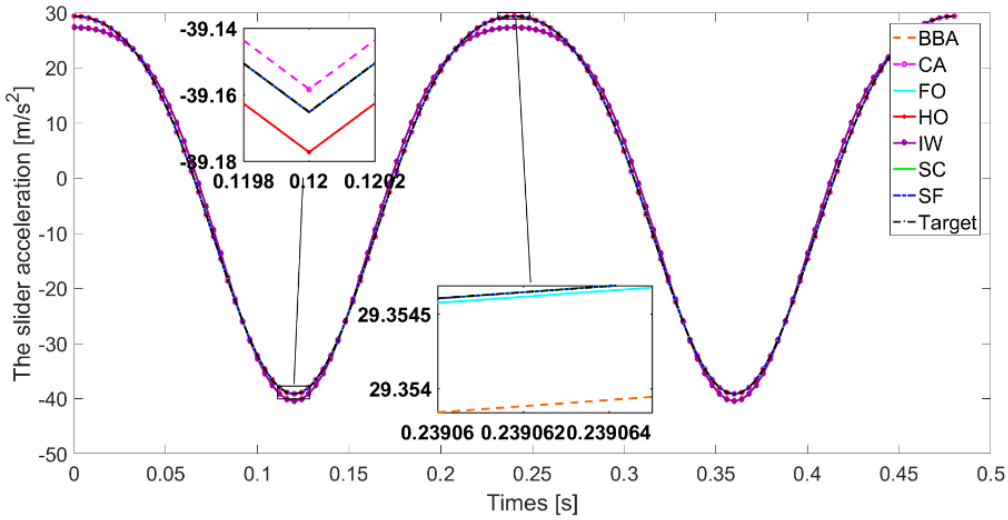

Figure 16: The slider acceleration responses based on the combined synthesis

Table 7 summarizes the proposed design variable parameters corresponding to all the involved techniques. It can be confirmed through the mechanism's responses that the combined synthesis did joy compromising all the responses. Thus, the optimal parameters of the mechanism don't dismiss any of the target responses to the detriment of another. As witnessed in Figure 15 for the slider velocity responses, the discrepancy is considerably reduced compared to the axial displacement synthesis. Moreover, all the optimization techniques' responses and the targets seem almost to be overlapped. Albeit, a zoom on Figure 15 reveals the existence of a slight mismatching. Similarly, to the slider velocity responses, the slider acceleration responses depicted in Figure 16 confirm an excellent fitting for the obtained results with the target. Thus, the gap witnessed in section 5.1 is considerably depleted. The analysis of Figure 17 for the flexible connecting-rod's axial displacement mid-point confirms the previous assertions. In contrast with the mono-objective optimization wherein only the involved response along the synthesis process is met, the combined optimization concludes a perfect trade-off for the three involved responses simultaneously.

Table 7: The combined error optimization results

	l_2(mm)	l_3(mm)	ρ(kg/m^3)	E (kPa)	b(mm)	h(mm)	Error
BBO	49.9993	349.9683	$2.4295\ 10^{3}$	$6.5282\ 10^{10}$	1.5255	26.5831	$1.3194\ 10^{-5}$
CA	49.9780	349.1120	$2.3646\ 10^{3}$	$7.3330\ 10^{10}$	1.4156	24.6997	$3.7418\ 10^{-4}$
FO	50.0000	349.9974	$2.6197\ 10^{3}$	$7.4992\ 10^{10}$	1.4781	22.8527	$3.5712\ 10^{-6}$
HO	50.0146	350.0620	$2.0119\ 10^{3}$	$6.8471\ 10^{10}$	1.3564	30.0000	$1.2746\ 10^{-4}$
IWO	49.4562	256.1265	$2.1660\ 10^{3}$	$7.1019\ 10^{10}$	1.0000	28.3616	$1.6033\ 10^{-2}$
SCE	50.0000	350.0000	$2.3908\ 10^{3}$	$7.1653\ 10^{10}$	1.4446	24.6296	$8.0657\ 10^{-9}$
SF	49.9999	349.9999	$2.7071\ 10^{3}$	$6.6852\ 10^{10}$	1.5914	24.0689	$5.9590\ 10^{-9}$

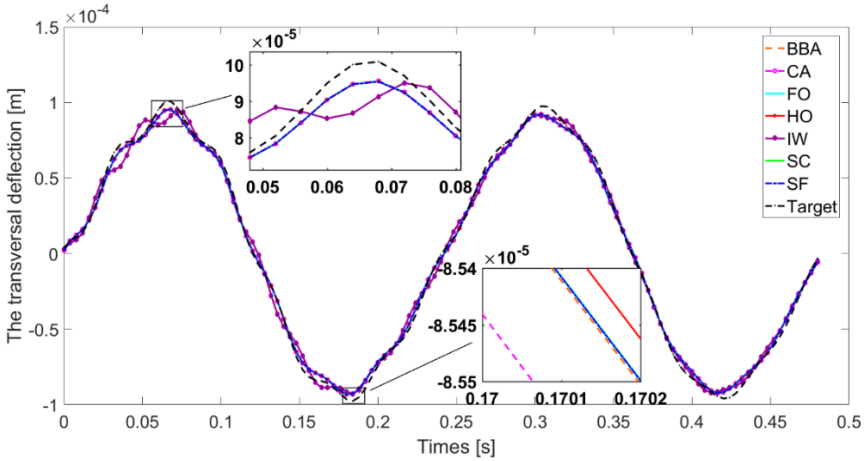

Figure 17: The axial displacement responses based on the combined synthesis

5.2. The four-bar mechanism synthesis

The second benchmark mechanism of scope in this work is a four-bar subsuming two flexible bodies, the connector and the follower. Five involved responses are backing-up the synthesis approach, namely, the crank, connector, and follower mid-point path as well as the axial displacement for both the connector and follower. The deployed responses represent a mix between some common responses used in previous works such as the connector mid-point path, but also cover some other uncommonly treated. The main reason behind considering similar responses is to ensure that the optimal design variables for the mechanism satisfy simultaneously, not only a single but all the mechanism's responses. A single based response synthesis could be valid for rigid mechanisms; however, the present case of study treats a compliant mechanism wherein two flexible components are instilled. Hence, satisfying a single response couldn't vow that all of them are, though. Consequently, for the four-bar mechanism, a set of responses have been involved simultaneously in the cost function. Moreover, other mechanisms could be associated with the four-bar mechanism, namely with whether the crank, connector, or follower mid-point. Since both the connector and follower are considered as flexible bodies, the axial displacement taking place could pull over the stretched path out of the target introducing consequently the mechanism in a completely different path. This leads to some disastrous consequences namely for medical application such as rehabilitation mechanism. Twelve design variables have been considered for the mechanism synthesis split between dimensional and characteristic parameters. The length of the different links as well the two flexible links, connector and follower, height, width, Young modulus and material density are of scope as detailed in the following design variable vector $X = [l_1 \quad l_2 \quad l_3 \quad l_4 \quad E_3 \quad \rho_3 \quad h_3 \quad a_3 \quad E_4 \quad \rho_4 \quad h_4 \quad a_4.]$. The optimal parameters are summarized in Table 8.

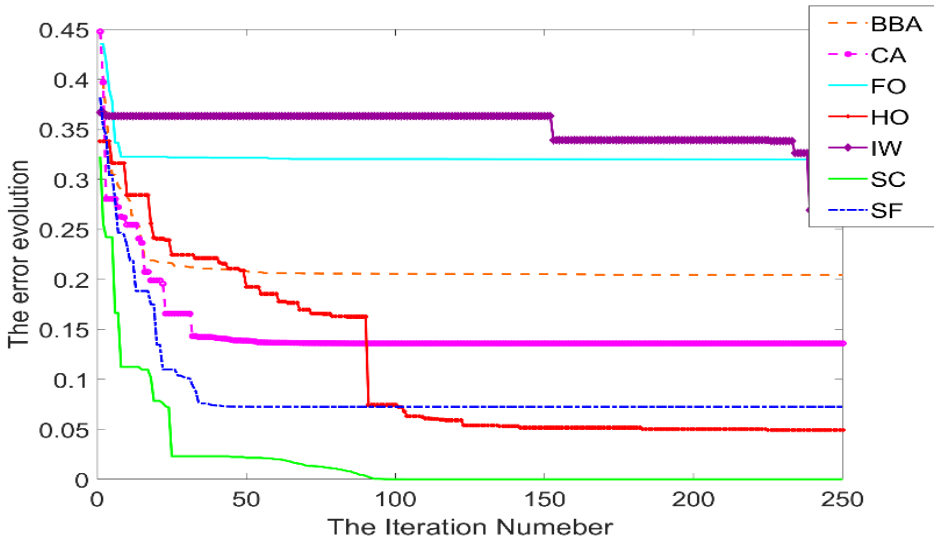

Figure 18: The error evolution

Involving the Young modulus and material density as design parameters could give the designer much more freedom to cope with a wider range of applications under different conditions.

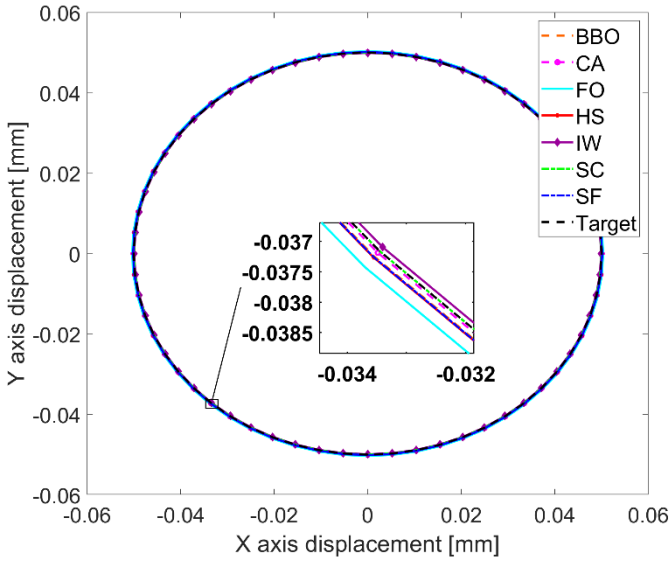

Figure 19: The crank mid-point path

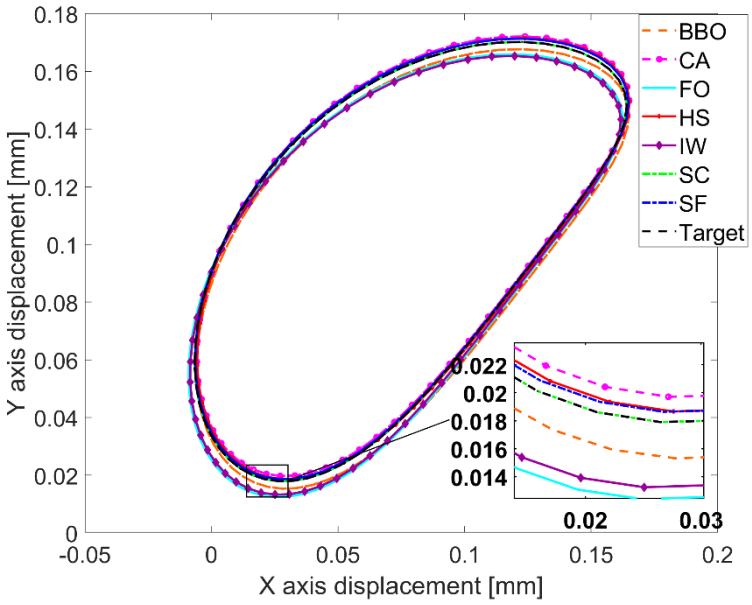

Figure 20: The connector mid-point path

As it can be inferred from Figure 18, the SC, SF, and HS techniques perform well for the four-bar mechanism. In perfect agreement with previous results for the slider-crank mechanism synthesis, the SC is leading the other techniques for all the synthesis types providing always the best solution. This confirms that a similar technique is auspicious for all synthesis types in tremendous industrial fields and applications.

The crank mid-point path depicted in Figure 19 confirms that the SC technique proposes a set of design variables perfectly fitting with the target response. However, similarly to most of the

slider-crank mechanism scenarios cases, the FO and BBO algorithms are burdened to satisfy the desired response.

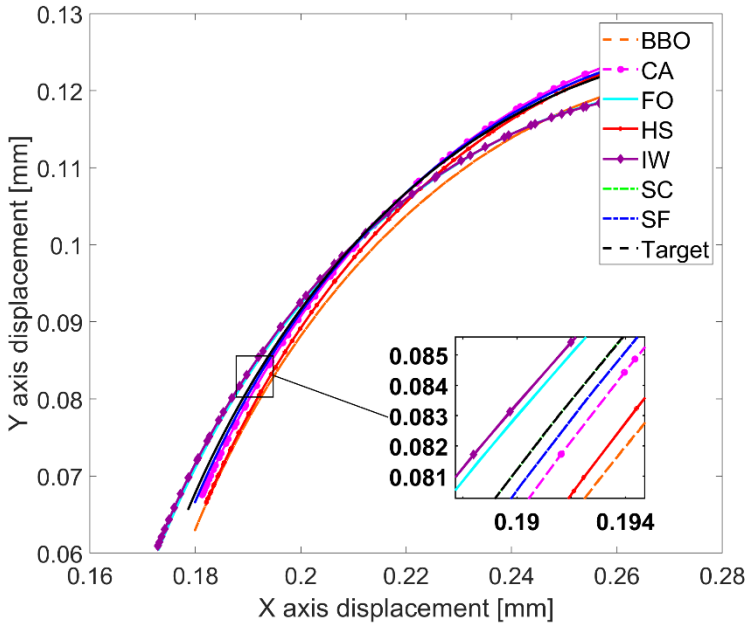

Figure 21: The follower mid-point path

The second response to be assessed is the connector mid-point path. As seen in Figure 20, the SC technique remains outstandingly performing the other techniques offering design variables perfectly matching with the target responses. The HS and SF as well cope well with the target connector mid-point path. For the remaining techniques, the already existing discrepancy for the crank mid-point path affects the connector mid-point path and stretch away from their paths for the connector mid-point.

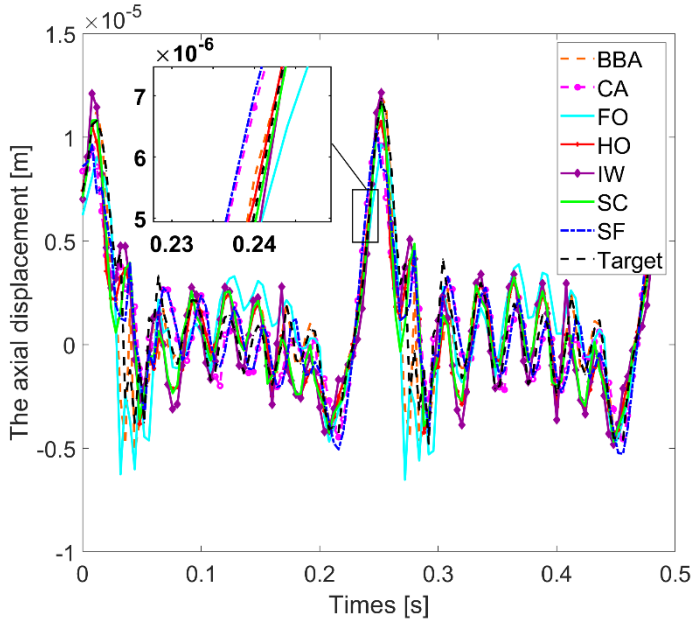

Figure 22: The connector mid-point axial displacement

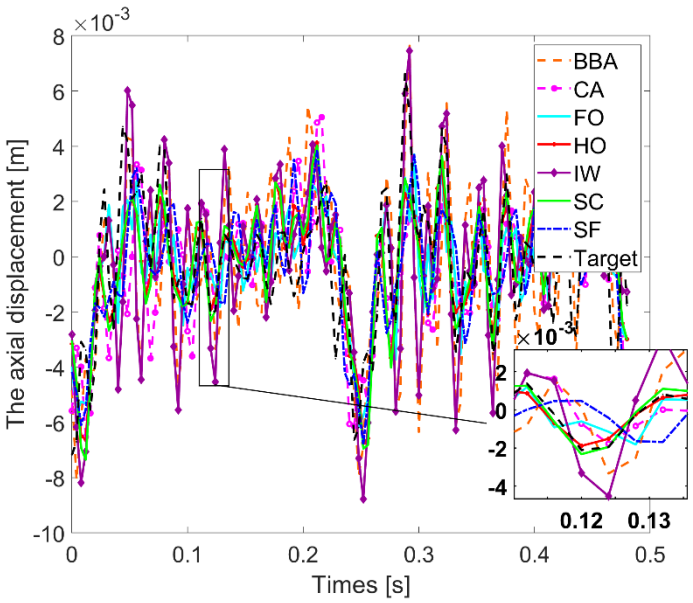

Figure 23: The follower mid-point axial displacement

Table 8: The four-bar optimal parameters for the set of optimization techniques

	l_1(mm)	l_2(mm)	l_3(mm)	l_4(mm)	E_3 (kPa)	ρ_3 (kg/m^3)	h_3(mm)	a_3 (mm)	E_4 (kPa)	ρ_4 (kg/m^3)	h_4(mm)	a_4 (mm)	Error
BBA	284.9357	100.2532	246.7922	244.8782	6.7636	2284.3676	1.4525	25.1765	6.8341	2419.9309	1.9249	24.9987	0.204418
CA	288.860	100.080	254.031	254.033	6.293	2440.298	1.551	26.205	6.865	2537.590	1.398	25.277	0.135884
FO	276.934	100.723	240.000	240.408	7.205	2999.209	1.999	21.929	7.343	2150.530	1.993	25.355	0.319613
HO	289.560	100.292	252.842	252.843	6.699	2076.070	1.534	23.560	6.584	2612.908	1.360	28.179	0.049148
IW	276.270	99.834	240	240	7.485	2229.824	1.406	23.861	6.643	2506.748	1	20	0.26932
SC	285	100	249.999	249.999	7.150	2248.561	1.4999	24	7.161	2831.591	1.323	27.029	1.973 e-11
SF	286.964	100.279	252.105	252.102	7.007	2961.311	1.532	23.701	6.773	2648.315	1.514	24.931	0.07254

The third response involved in the cost function (eq 25) for the four-bar mechanism synthesis is the follower mid-point path. Following the drawn paths in Figure 21, perfect matching for the target response could be inferred for the SC technique. Similar to the connector mid-point path, the HS and SF are of acceptable accuracy. In order to better understand the origin of the

discrepancy emerging between the target and obtained responses for the set of optimization techniques, an analysis of the axial displacement taking place in the two considered flexible components is carried out. The axial displacement of the connector mid-point taking place (Figure 22) is almost similar to the target one for the SC. This justifies the fact that the design parameters for this technique satisfy perfectly the desired path for the connector. Moreover, the analysis of the follower mid-point axial displacement confirms that for the SC technique the axial displacement almost overlaps the target one as depicted in Figure 23. It could be inferred also that both the HS and SF techniques provide similar responses to the target ones in terms of axial displacement.

6. Statistical analysis

Table 9 : Friedman test and critical difference of Bonferroni–Dunn test

	Friedman mean rank	Rank
BBA	**3.75**	**4**
CA	**2.25**	**1**
FO	**5.25**	**7**
HO	**3.25**	**3**
IW	**4.75**	**6**
SC	**3**	**2**
SF	**4**	**5**

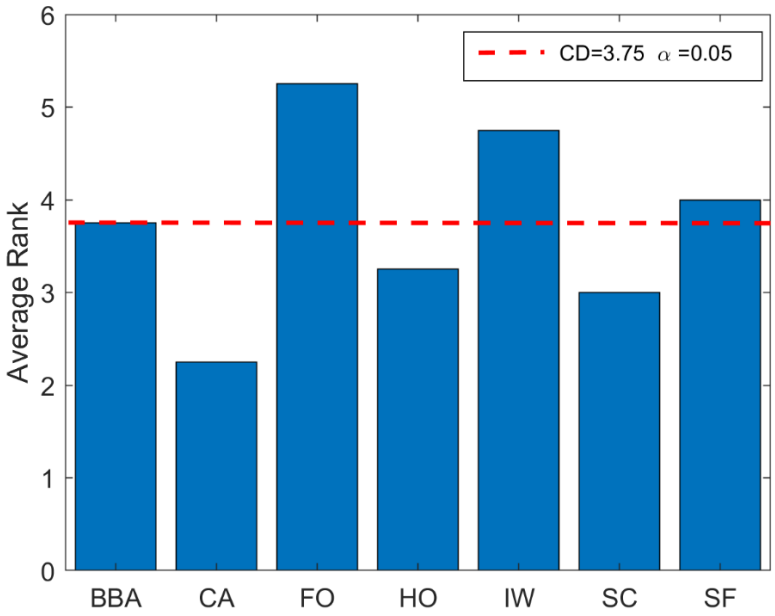

Figure 24 : Friedman test and Bonferroni–Dunn's test for different algorithms for α = 0.05

A statistical analysis based on Friedman [49,50] test has been carried out to investigate the performance of the algorithms. In order to emphasize which of the algorithms outstandingly performs compared to the others, a ranking based on the Friedman test and critical difference of Bonferroni–Dunn test has been established as detailed in Table 9. It could be inferred that among all the techniques, the Cultural Algorithm (CA) outperform the other algorithms as it is ranked at the first position as witnessed in

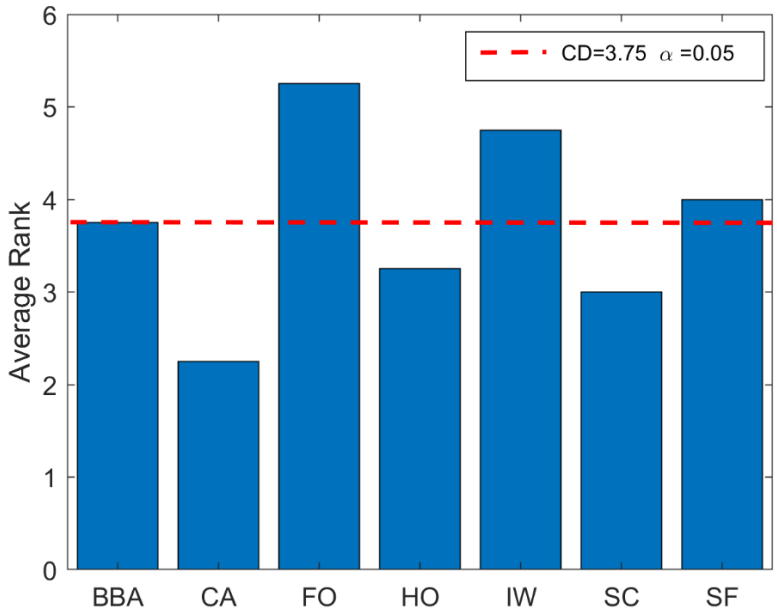

Figure 24. The average ranking is based on one significance level of 0.05. The red cut-line in

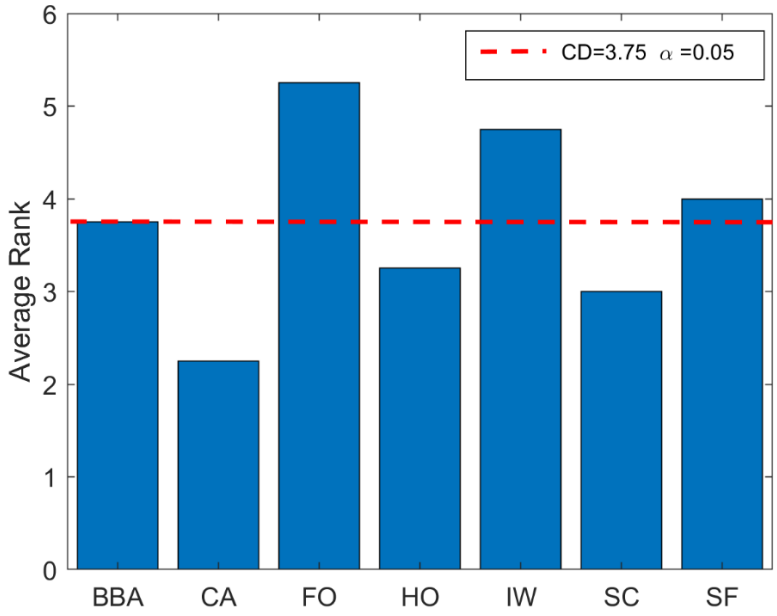

Figure 24 depicts that the sum of the ranking of the Cultural Algorithm (CA) is equal to the significance level. The results confirm that three of the deployed algorithms are beyond the threshold, namely, the FO, IW and SF.

7. Conclusions

This work denotes an insight into a compliant mechanism synthesis. Two illustrative examples have been investigated, mainly, flexible slider-crank and flexible four-bar mechanisms. Six design variables for the mechanism dimensions and material characteristics have been of scope for the flexible slider-crank mechanism. Whereas, twelve parameters have been of interest for the flexible four-bar mechanism. Seven optimization techniques have been used for the mechanism synthesis based on whether a dynamic response, a drawn path, or a flexible midpoint axial displacement. The proposed synthesis approach efficiency has been investigated. Some important conclusions could be drawn namely, the SC technique proposes high accuracy solutions for a single synthesis-based response. For the combined synthesis, all the responses involved are satisfied concluding a perfect trade-off between them. The proposed approach in this work can propose, for the designer, a set of solutions for the synthesis problem based on non-common responses namely dynamic responses or a flexible body axial displacement considering the material characteristics such as Young modulus and material density. It should be highlighted that for flexible mechanisms, a single-based response synthesis satisfies only the involved one. Whereas, the mechanism remaining responses are dismissed. In order to obtain accurate results, it is recommended to deploy the combined synthesis approach. It is interesting to extend the present work for other mechanisms such as robot arms and exoskeleton. Including clearance into the mechanical joints alongside flexible bodies is also of scope in future works.

References

[1] P. Flores, J. Ambrósio, J.C.P. Claro, H.M. Lankarani, Dynamic behaviour of planar rigid multi-body systems including revolute joints with clearance, Proc. Inst. Mech. Eng. Part K J. Multi-Body Dyn. 221 (2007) 161–174. https://doi.org/10.1243/14644193jmbd96.

[2] S. Bai, J. Angeles, Coupler-curve synthesis of four-bar linkages via a novel formulation, Mech. Mach. Theory. 94 (2015) 177–187. https://doi.org/10.1016/j.mechmachtheory.2015.08.010.

[3] S.M. Han, S. In Kim, Y.Y. Kim, Topology optimization of planar linkage mechanisms for path generation without prescribed timing, Struct. Multidiscip. Optim. 56 (2017) 501–517. https://doi.org/10.1007/s00158-017-1712-6.

[4] Y. Shao, Z. Xiang, H. Liu, L. Li, Conceptual design and dimensional synthesis of cam-linkage mechanisms for gait rehabilitation, Mech. Mach. Theory. 104 (2016) 31–42. https://doi.org/10.1016/j.mechmachtheory.2016.05.018.

[5] S. Ebrahimi, P. Payvandy, Efficient constrained synthesis of path generating four-bar mechanisms based on the heuristic optimization algorithms, Mech. Mach. Theory. 85 (2015) 189–204. https://doi.org/10.1016/j.mechmachtheory.2014.11.021.

[6] V. Parlaktaş, E. Söylemez, E. Tanik, On the synthesis of a geared four-bar mechanism, Mech. Mach. Theory. 45 (2010) 1142–1152. https://doi.org/10.1016/j.mechmachtheory.2010.03.007.

[7] S. Hadizadeh Kafash, A. Nahvi, Optimal synthesis of four-bar path generator linkages using Circular Proximity Function, Mech. Mach. Theory. 115 (2017) 18–34. https://doi.org/10.1016/j.mechmachtheory.2017.04.010.

[8] G. Ganesan, M. Sekar, Optimal synthesis and kinematic analysis of adjustable four-bar linkages to generate filleted rectangular paths, Mech. Based Des. Struct. Mach. 45 (2017) 363–379. https://doi.org/10.1080/15397734.2016.1217780.

[9] V. Van Der Wijk, The Grand 4R Four-Bar Based Inherently Balanced Linkage Architecture for synthesis of shaking force balanced and gravity force balanced mechanisms, 150 (2020). https://doi.org/10.1016/j.mechmachtheory.2020.103815.

[10] A. Hernández, A. Muñoyerro, M. Urízar, E. Amezua, Comprehensive approach for the dimensional synthesis of a four-bar linkage based on path assessment and reformulating the error function, 156 (2021). https://doi.org/10.1016/j.mechmachtheory.2020.104126.

[11] Y. Shao, W. Zhang, X. Ding, Configuration synthesis of variable stiffness mechanisms based on guide-bar mechanisms with length-adjustable links, Mech. Mach. Theory. 156 (2021) 104153. https://doi.org/10.1016/j.mechmachtheory.2020.104153.

[12] S. Bai, Algebraic coupler curve of spherical four-bar linkages and its applications, Mech. Mach. Theory. 158 (2021) 104218. https://doi.org/10.1016/j.mechmachtheory.2020.104218.

[13] K. Xu, H. Liu, W. Yue, J. Xiao, Y. Ding, G. Wang, Kinematic modeling and optimal design of a partially compliant four-bar linkage using elliptic integral solution, 157 (2021) 13–14. https://doi.org/10.1016/j.mechmachtheory.2020.104214.

[14] A. Yildiz, Parametric synthesis of two different trunk lid mechanisms for sedan vehicles using population-based optimisation algorithms, Mech. Mach. Theory. 156 (2021) 104130. https://doi.org/10.1016/j.mechmachtheory.2020.104130.

[15] M. Olinski, A. Gronowicz, M. Ceccarelli, Development and characterisation of a controllable adjustable knee joint mechanism, 155 (2021) 1–14. https://doi.org/10.1016/j.mechmachtheory.2020.104101.

[16] J.F. Collard, P. Duysinx, P. Fisette, Optimal synthesis of planar mechanisms via an extensible-link approach, Struct. Multidiscip. Optim. 42 (2010) 403–415. https://doi.org/10.1007/s00158-010-0500-3.

[17] V. Venkataramanujam, P.M. Larochelle, Design and development of planar reconfigurable motion generators, Mech. Based Des. Struct. Mach. 44 (2016) 426–439. https://doi.org/10.1080/15397734.2015.1096794.

[18] W.Y. Lin, K.M. Hsiao, A new differential evolution algorithm with a combined mutation strategy for optimum synthesis of path-generating four-bar mechanisms, Proc. Inst. Mech. Eng. Part C J. Mech. Eng. Sci. 231 (2017) 2690–2705. https://doi.org/10.1177/0954406216638887.

[19] J. Brinker, B. Corves, Y. Takeda, Parallel Robots Based on Motion / Force Transmission Indices, Mech. Mach. Theory. 0 (2018) 1–15. https://doi.org/10.1016/j.mechmachtheory.2017.11.029.

[20] J. Sun, P. Wang, W. Liu, J. Chu, Non-integer-period motion generation of a planar four-bar mechanism using wavelet series, 121 (2018) 28–41.

[21] R. Alizade, E. Gezgin, Synthesis of function generating spherical four bar mechanism

for the six independent parameters, Mech. Mach. Theory. 46 (2011) 1316–1326. https://doi.org/10.1016/j.mechmachtheory.2011.04.002.

[22] R. Wu, R. Li, S. Bai, A fully analytical method for coupler-curve synthesis of planar four-bar linkages, 155 (2021). https://doi.org/10.1016/j.mechmachtheory.2020.104070.

[23] Y. Liu, R. Bucknall, A survey of formation control and motion planning of multiple unmanned vehicles, Robotica. 36 (2018) 1019–1047. https://doi.org/10.1017/s0263574718000218.

[24] T. Zhang, W. Zhang, M.M. Gupta, An underactuated self-reconfigurable robot and the reconfiguration evolution, Mech. Mach. Theory. 124 (2018) 248–258. https://doi.org/10.1016/j.mechmachtheory.2018.03.004.

[25] S. Botello-Aceves, S.I. Valdez, H.M. Becerra, E. Hernandez, Evaluating concurrent design approaches for a Delta parallel manipulator, Robotica. 36 (2018) 697–714. https://doi.org/10.1017/s0263574717000674.

[26] R. Roberts, E. Rodriguez-Leal, Kinematics and workspace-based dimensional optimization of a novel haptic device for assisted navigation, Mech. Based Des. Struct. Mach. 44 (2016) 43–57. https://doi.org/10.1080/15397734.2015.1035784.

[27] S.I. Valdez, E. Chávez-Conde, E.E. Hernandez, M. Ceccarelli, Structure-control design of a mechatronic system with parallelogram mechanism using an estimation of distribution algorithm, Mech. Based Des. Struct. Mach. 44 (2016) 58–71. https://doi.org/10.1080/15397734.2015.1035785.

[28] A. Hernández, A. Muñoyerro, M. Urízar, E. Amezua, Comprehensive approach for the dimensional synthesis of a four-bar linkage based on path assessment and reformulating the error function, Mech. Mach. Theory. 156 (2021) 104126. https://doi.org/https://doi.org/10.1016/j.mechmachtheory.2020.104126.

[29] J.K. Pickard, J.A. Carretero, J.-P. Merlet, Appropriate synthesis of the four-bar linkage, Mech. Mach. Theory. 153 (2020) 103965. https://doi.org/https://doi.org/10.1016/j.mechmachtheory.2020.103965.

[30] M.R. Haghjoo, J. Yoon, Two-stage mechanism path synthesis using optimized control of a shadow robot: Case study of the eight-bar Jansen mechanism, Mech. Mach. Theory. 168 (2022) 104569. https://doi.org/https://doi.org/10.1016/j.mechmachtheory.2021.104569.

[31] V. van der Wijk, The Grand 4R Four-Bar Based Inherently Balanced Linkage Architecture for synthesis of shaking force balanced and gravity force balanced mechanisms, Mech. Mach. Theory. 150 (2020) 103815. https://doi.org/https://doi.org/10.1016/j.mechmachtheory.2020.103815.

[32] J.L. Torres-Moreno, N.C. Cruz, J.D. Álvarez, J.L. Redondo, A. Giménez-Fernandez, An open-source tool for path synthesis of four-bar mechanisms, Mech. Mach. Theory. 169 (2022) 104604. https://doi.org/https://doi.org/10.1016/j.mechmachtheory.2021.104604.

[33] P.E. Nikravesh, Computer-Aided Analysis of Mechanical Systems, 1988.

[34] P. Flores, J. Ambrósio, J.P. Claro, Dynamic analysis for planar multibody mechanical

systems with lubricated joints, Multibody Syst. Dyn. 12 (2004) 47–74. https://doi.org/10.1023/B:MUBO.0000042901.74498.3a.

[35] A.A. Shabana, Dynamics of Multibody Systems, Fourth Edi, 2013.

[36] A.A. SHABANA, Computational Dynamics, 2010. https://doi.org/10.1002/9780470686850.

[37] L. Romdhane, H. Dhuibi, H. Hadj Salah, Dynamic analysis of planar elastic mechanisms using the dyad method, Proc. Inst. Mech. Eng. Part K J. Multi-Body Dyn. 217 (2003) 1–14. http://dx.doi.org/10.1243/146441903763049397.

[38] George N.S. Arthur G. Erdman, Advanced mechanism design: analysis and synthesis volume 2, 1988. https://doi.org/10.1073/pnas.0703993104.

[39] J.A. Cabrera, A. Simon, M. Prado, Optimal synthesis of mechanisms with genetic algorithms, Mech. Mach. Theory. 37 (2002) 1165–1177. https://doi.org/10.1016/S0094-114X(02)00051-4.

[40] M.. Laribi, A. Mlika, L. Romdhane, S. Zeghloul, A combined genetic algorithm–fuzzy logic method (GA–FL) in mechanisms synthesis, Mech. Mach. Theory. 39 (2004) 717–735. https://doi.org/10.1016/j.mechmachtheory.2004.02.004.

[41] I. Khemili, L. Romdhane, Dynamic analysis of a flexible slider-crank mechanism with clearance, Eur. J. Mech. A/Solids. 27 (2008) 882–898. https://doi.org/10.1016/j.euromechsol.2007.12.004.

[42] I. Khemili, M.A. Ben Abdallah, N. Aifaoui, Multi-objective optimization of a flexible slider-crank mechanism synthesis, based on dynamic responses, Eng. Optim. (2018). https://doi.org/10.1080/0305215X.2018.1508574.

[43] D. Simon, Biogeography-based optimization, IEEE Trans. Evol. Comput. 12 (2008) 702–713. https://doi.org/10.1109/TEVC.2008.919004.

[44] H.C. Kuo, C.H. Lin, Cultural evolution algorithm for global optimizations and its applications, J. Appl. Res. Technol. 11 (2013) 510–522. https://doi.org/10.1016/S1665-6423(13)71558-X.

[45] X. Yang, Nature-Inspired Metaheuristic Algorithms Second Edition, 2010. https://doi.org/10.1016/j.chemosphere.2009.08.026.

[46] Z.W. Geem, J.H. Kim, G. V Loganathan, A New Heuristic Optimization Algorithm: Harmony Search, Simulation. 76 (2001) 60–68. https://doi.org/10.1177/003754970107600201.

[47] A.R. Mehrabian, C. Lucas, A novel numerical optimization algorithm inspired from weed colonization, Ecol. Inform. 1 (2006) 355–366. https://doi.org/10.1016/j.ecoinf.2006.07.003.

[48] J.W. Kim, T.W. Seo, J. Kim, A new design methodology for four-bar linkage mechanisms based on derivations of coupler curve, Mech. Mach. Theory. 100 (2016) 138–154. https://doi.org/10.1016/j.mechmachtheory.2016.02.006.

[49] B. Firouzi, A. Abbasi, P. Sendur, Improvement of the computational efficiency of

metaheuristic algorithms for the crack detection of cantilever beams using hybrid methods, Eng. Optim. (2021) 1–22. https://doi.org/10.1080/0305215X.2021.1919887.

[50] S. García, D. Molina, M. Lozano, F. Herrera, A study on the use of non-parametric tests for analyzing the evolutionary algorithms' behaviour: a case study on the CEC'2005 Special Session on Real Parameter Optimization, J. Heuristics. 15 (2008) 617. https://doi.org/10.1007/s10732-008-9080-4.